Capillary suspensions as beneficial formulation concept for high energy density Li-ion battery electrodes

CrossMark

Boris Bitsch [a, *], Tobias Gallasch [b], Melanie Schroeder [b], Markus Börner [b], Martin Winter [b, c], Norbert Willenbacher [a]

[a] Karlsruhe Institute of Technology, Institute for Mechanical Process Engineering and Mechanics, Gotthard-Franz-Str. 3, 76131 Karlsruhe, Germany
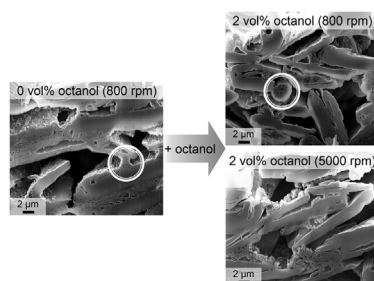[b] University of Münster, MEET Battery Research Center, Corrensstr. 46, 48149 Münster, Germany
[c] Helmholtz-Institute Münster, IEK 12, Forschungszentrum Jülich GmbH, Corrensstr. 46, 48149 Münster, Germany

HIGHLIGHTS

- Adjusting the electrode microstructure is achievable using capillary suspensions.
- Electrodes with staged porosity were fabricated showing excellent cycling behavior.
- Double layer electrodes were prepared without additional processing steps.

GRAPHICAL ABSTRACT

ABSTRACT

We introduce a novel formulation concept to prepare high capacity graphite electrodes for lithium ion batteries. The concept is based on the capillary suspension phenomenon: graphite and conductive agent are dispersed in an aqueous binder solution and the organic solvent octanol is added as immiscible, secondary fluid providing the formation of a sample-spanning network resulting in unique stability and coating properties. No additional processing steps compared to conventional slurry preparation are required. The resulting ultra-thick electrodes comprise mass loadings of about 16.5 mg cm^{-2}, uniform layer thickness, and superior edge contours. The adjustment of mechanical energy input ensures uniform distribution of the conductive agent and sufficient electronic conductivity of the final dry composite electrode. The resulting pore structure is due to the stable network provided by the secondary fluid which evaporates residue-free during drying. Constant current-constant potential (CC-CP) cycling clearly indicates that the corresponding microstructure significantly improves the kinetics of reversible Li$^+$ (de-) intercalation. A double layer electrode combining a conventionally prepared layer coated directly onto the Cu current collector with an upper layer stabilized with octanol was prepared applying wet-on-wet coating. CC-CP cycling data confirms that staged porosity within the electrode cross section results in superior electrochemical performance.

© 2016 Elsevier B.V. All rights reserved.

1. Introduction

High energy density lithium ion batteries (LIBs) for stationary applications are supposed to be manufactured cost efficient in

* Corresponding author.
E-mail address: boris.bitsch@kit.edu (B. Bitsch).

order to contribute substantially to a renewable energy based electrical energy supply system [1,2]. This task requires the use of robust and cheap electrode materials as well as innovative and simple processing routines focusing on aqueous electrode formulations [3–9]. One approach is to fabricate ultra-thick electrodes with high mass loadings to reduce the amount of inactive material like current collectors and separators for a given cell volume. However, for long cycle and calendar life as well as for superior electrochemical performance sufficient mechanical layer strength and electronic conductivity properties are essential [10,11]. As a major drawback, high mass loading and dry film thickness have been reported to decelerate lithium ion transport rates. The inhomogeneous electrolyte penetration and therefore incomplete utilization of the active material within such electrodes increases the irreversible capacity [12]. Furthermore, poor adhesion between the composite electrode consisting of active material, conductive agent, very often carbon blacks [13–15], binder and the current collector as well as poor interfacial electron transport properties increase the impedance of the battery cell resulting in poor rate performance and electrode kinetics (Li ion transport limitation) [16]. Impedance spectroscopy based on suitable equivalent circuit models has been used to quantify e.g. the influence of pore structure and porosity on Li ion transport properties [17–22]. Transport kinetics is strongly correlated to the electrode microstructure, i.e. the distribution of active material, conductive agent as well as binder and the resulting pore size distribution depending on mixing and preparation procedures [12,23–26]. Especially in case of ultra-thick electrodes lithium ion transport limitations play a significant role [27,28] but might be overcome by creation of an adjusted pore structure. From a kinetics point of view a porosity gradient across the electrode with an increased porosity at the electrode surface adjacent to the separator allowing for fast ion transport and a compact layer close to the current collector to ensure optimum electronic contact would be preferential [29,30].

Generally, the porosity and pore size distribution of a particulate dried layer fabricated from a suspension depend on shape and size distribution of the utilized solid components. Commonly, with decreasing mean particle size the bulk density increases [31], i.e. the layer porosity drops. Furthermore, multimodal particle distributions result in higher bulk density compared to monomodal particle distributions [31]. Following these considerations, an approach to fabricate electrodes with a porosity gradient could be a multilayer coating with electrode slurries having particles with varied mean particle size [30]. Reduced diffusion path lengths and ohmic resistances resulting in higher capacities and power densities have been achieved using 3D microstructured electrodes [32–34]. However, from a processing perspective the generation of 3D microstructures is expensive and involves additional complex fabrication steps. Aiming at an industrial scale, electrode fabrication using established processing equipment, a minimum number of processing steps would be preferential.

In a previous study, we have introduced an aqueous anode slurry formulation concept based on the so-called capillary suspension phenomenon [35] and we could show that the observed unique rheological properties of capillary suspensions resulted in improved processing and coating behavior [36]. The dry composite electrodes investigated in this study were calendared to obtain similar porosity thus avoiding effects resulting from morphology deviations of electrodes based on regular slurries as well as capillary suspensions. However, the capillary suspension concept offers a smart approach to tune the microstructure of particulate matter in a targeted manner and has already been successfully applied to fabricate highly porous ceramic and glassy membranes [37–40].

In this work, we apply the capillary suspension concept to process graphite anodes [41] with adjustable and even staged porosity in order to improve the overall lithium ion transport kinetics. The influence of the microstructure on lithium ion transport properties is investigated in detail to evaluate concepts for a further targeted electrode development. Exemplarily, octanol is used as secondary processing fluid and structuring agent. Since octanol evaporates residue-free during drying [36], this additive can easily be implemented into the standard processing routine. Electrodes with staged porosity are obtained using a double-layer slot-die coater to deposit a conventional electrode slurry onto the current collector and a capillary suspension based slurry on top of it.

Beyond this, the capillary suspension concept offers additional opportunities, e.g. for an efficient, targeted deposition of the binder using the secondary fluid as carrier [40], but this is dedicated to future research.

2. Experimental

2.1. Materials, slurry preparation and electrode coating

Commercially available plate-shaped, synthetic graphite powder (SLP30, Imerys Graphite & Carbon, Bodio, Switzerland) with a volume-based average diameter $d_{50} = 16$ µm, a specific surface area of 8.0 $m^2\,g^{-1}$ and a density of 2.3 $g\,cm^{-3}$ was used as active material for aqueous anode slurry preparation. Compared to a carbon powder consisting of micro beads or spherical granules, an active material that consists of plate-shaped particles is more suitable to prepare thick composite electrodes since sufficient electric conductivity of more densely packed layers is anticipated. These layer properties are supposed to facilitate a successful electrochemical characterization of ultra-thick composite electrodes. Carbon black (CB, Super P Li, Imerys Graphite & Carbon) with a density of 1.8 $g\,cm^{-3}$ was added as conductive agent. The size of the primary CB particles varies between 20 nm and 40 nm, but in the slurry these particles are typically present as agglomerates with an average size of several microns [42]. Sodium carboxymethylcellulose (CMC, Dow Wolff Cellulosics GmbH, Bomlitz, Germany) with a density of 1.6 $g\,cm^{-3}$ and a Brookfield viscosity of about 2.2 Pa s (2 wt% aqueous solution at 25 °C) was used as binder and rheology control agent. The solids content was kept constant at 20 vol% and the weight ratio of active material, conductive agent and binder was 91.9:5.1:3.0 (graphite:CB:CMC) referring to the dry composite electrode for all experiments. After homogeneous dispersion of all solids in the aqueous binder solution, 1-octanol (Alfa Aesar, Karlsruhe, Germany) with a density of 0.83 $g\,cm^{-3}$ and dynamic viscosity of 9 mPa s (at 20 °C) was added as secondary fluid at concentrations up to 2 vol%.

For slurry preparation CMC was dissolved in distilled water (3 wt%, CMC-H_2O mixture) and homogenized with a propeller mixer (mixing unit: Dispermat AE03-C1, VMA-Getzmann, Reichshof, Germany). Carbon black and graphite powder were dispersed in the homogenous CMC-water solution using a dissolver disk (57 mm in diameter) at 1200 rpm for 50 min. To ensure particle deagglomeration and excellent slurry homogeneity a suspension with high solids content (32 vol%) was initially mixed while the amount of water was raised stepwise with time until reaching a final solids content of 20 vol% and a CMC concentration of 0.83 vol% [43]. The rotational speed after addition of octanol to the suspension was varied. Therefore, dissolver mixing after octanol addition was performed at differing rotational speed between 800 rpm and 8000 rpm for 300 s. Fig. 1 summarizes the slurry processing procedure in more detail and displays the solids concentration as a function of mixing time.

Slurries were coated on copper foil (Itochu Corporation, Tokyo, Japan, 10 µm in thickness) using a doctor blade (ZUA 2000, Zehntner GmbH, Sissach, Switzerland) with a coating width of
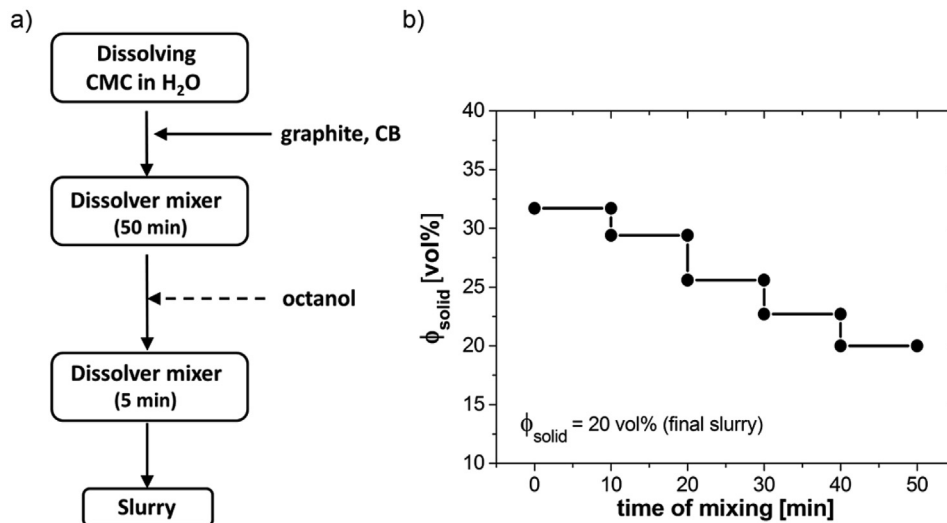
Fig. 1. Scheme of the slurry preparation process (a). Slurry mixing procedure: solid volume fraction as a function of mixing time to illustrate the dilution steps (b).

60 mm and gap width of up to 600 μm whereas the mass loading was adjusted to about 16.5 mg cm^{-2}. In case of double layer coating different layers were slot die coated on top of each other in the wet state. For layer conductivity measurements glass plates were used as substrate. Subsequently, all electrode layers were dried at 60 °C overnight in a drying chamber at ambient atmosphere.

For half-cell preparation and subsequent electrochemical cycling both electrode and pure lithium metal sheets were punched in disks (12 mm in diameter). The graphite based anode layer was finally dried under vacuum at 80 °C for at least 12 h prior to cell assembly in an argon filled glove box. In Swagelok type half cells, graphite anodes and lithium metal sheets (counter and reference electrodes) were separated by polypropylene (PP) based separators (Freudenberg FS 2190, Freudenberg Vliesstoffe SE & Co. KG, Weinheim, Germany). A standard liquid electrolyte system (BASF SE, Ludwigshafen, Germany) consisting of ethylene carbonate (EC), dimethyl carbonate (DMC) and LiPF$_6$ (EC:DMC 1:1 by weight, 1 M LiPF$_6$) was used for cell preparation.

2.2. Analytical methods

2.2.1. Slurry rheology
Rheological slurry properties were measured using a stress-controlled rotational rheometer (RheoStress 1, Thermo Scientific, Karlsruhe, Germany) with a plate/plate geometry (diameter: 35 mm, gap height: 1 mm). The viscosity functions were determined applying shear stress ramps (initial stress: 0.5 Pa or 0.8 Pa, final stress: 500 Pa or 800 Pa, measurement time: 300 s, logarithmic stress slope: 1 decade per 100 s).

2.2.2. Electronic conductivity measurements and microstructural investigation
The layer conductivity of dried electrodes coated on glass plates was determined applying four-point conductivity measurements. Scanning electron microscopy (SEM) was used to investigate the morphology of the electrode surface with special attention to the CB distribution. To obtain an overview of the complete electrode cross-section the samples were embedded with epoxy resin (Struers Epofix) in a vertical position. After a curing time of about 12 h the samples were cut with a precision cutting machine (Struers Accutom-5) to obtain plane surfaces on both sides. The subsequent polishing was performed with an anhydrous lubricant

(Struers DP Blue) in four steps with different polishing cloths (Si-C paper, 2× woven acetate cloths, synthetic short nap) and abrasives containing diamond particles with averaged sizes of 9 μm, 3 μm and 1 μm, respectively. All consumables were purchased from Struers GmbH (Willich, Germany).

Additional electrode cross-sections were prepared by a focused ion beam (FIB) milling process to investigate the microstructure and especially the CB distribution in detail. The gallium ions were extracted from a high brightness liquid metal ion source. Furthermore, the region of interest was coated with a thin platinum layer to protect the surface using a gas injection system (GIS) prior to the FIB milling process. The samples were analyzed with an Auriga Crossbeam workstation (Carl Zeiss AG, Oberkochen, Germany) using an acceleration voltage of 3 kV for FIB-prepared cross-section and surface analysis and 15 kV for embedded samples.

The pore size distribution was measured by mercury intrusion porosimetry using a CEI Pascal 1.05 (Thermo Scientific Porotec Pascal 440 Series (high pressure region) and 140 Series (low pressure region)) operating in a pressure range up to 400 MPa. The relative porosity P can be calculated via $P = V_p/(V_p + 1/\rho)$ where V_P is the measured specific pore volume [cm^3 g^{-1}] and $\rho = \sum w_i \rho_i$ [g cm^{-3}] represents the density of the solid composite material. The latter value can be seen as a sum covering all electrode components in which each contribution ρ_i is normalized by the corresponding weight fraction w_i.

2.2.3. Electrochemical characterization
Constant current-constant potential (CC-CP) cycling experiments were performed in the potential range between 0.02 V and 1.50 V vs. Li/Li$^+$ for several cycles using a Maccor Series 4000 Battery Tester (Maccor Inc., Tulsa, USA). Lithium metal served as counter and reference electrodes in a T-type three electrode configuration. The cycling procedure comprises three formation cycles at a discharge rate of 0.1 C, followed by twelve cycles at 0.2 C and 20 cycles at 0.5 C. The corresponding current densities were determined to be (0.70 ± 0.04) mA cm^{-2}, (1.38 ± 0.07) mA cm^{-2} and (3.50 ± 0.20) mA cm^{-2} for 0.1 C, 0.2 C and 0.5 C, respectively. The applied current densities were calculated considering 91.9 wt% of the electrode material to be electrochemically active. In order to estimate the recovering ability of the electrodes three final cycles were carried out at 0.1 C. Independent of the constant current C-rate, constant potential steps were implemented at 0.02 V vs. Li/Li$^+$

until a remaining current density of 0.02 C was reached as cut-off criterion. For the double layer electrode constant potential steps were implemented at 0.02 V vs. Li/Li$^+$ until a remaining current density of 0.05 C was reached as cut-off criterion.

There are slight deviations in electrode mass loadings (± 0.5 mg cm^{-2}) that are insignificant regarding their influence on the electrochemical anode performance since only low-to-medium rate cycling is performed.

3. Results and discussion

3.1. Rheological characterization

Shear viscosity data for slurries including different amount of octanol are shown in Fig. 2. Obviously, the addition of this secondary fluid results in a strong increase of low shear viscosity (more than one order of magnitude at $\dot{\gamma} < 0.1$ s^{-1}). This stabilizes the slurry with respect to unwanted phase separation and sedimentation and in coating operation itself, it provides improved shape accuracy [36]. The increase in viscosity is very steep in the concentration range between 0.5 vol% and 1 vol% octanol and levels off at higher secondary fluid content. In contrast, the viscosity at high shear rates ($\dot{\gamma} > 50$ s^{-1}) relevant for processing or coating operations is essentially unaffected by the added fluid. Similar behavior has been observed for numerous ternary solid/fluid/fluid combinations [35,44] and could be attributed to the strong capillary forces acting among particles inferred by the added secondary fluid. In the ternary system investigated here octanol is the preferential wetting fluid and accordingly so-called pendular bridges between adjacent particles are formed resulting in a percolating, sample-spanning network [45]. When strong hydrodynamic stresses act, i.e. at high shear rates, the network breaks down and the secondary fluid does not affect the viscosity typically relevant during processing. Fast network recovery even after high energy input [46] guarantees high shape accuracy and formation of coated layers with uniform thickness [26]. During drying the capillary bridges in such ternary suspensions prevent the collapse and densification of the particle structure. This phenomenon has been used to fabricate highly porous ceramic, glassy, polymeric, and also self-supporting graphite membranes [37—40]. Here it will be used to control the porosity of the electrode layers as will be discussed in detail below.
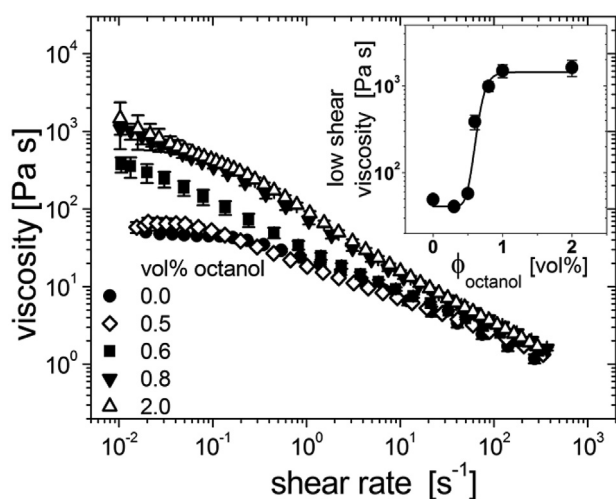

Fig. 2. Viscosity as a function of shear rate for slurries prepared with different octanol content. The insert shows the low shear viscosity at a fixed shear rate of $\dot{\gamma} = 0.01$ s^{-1} as a function of the octanol concentration.

3.2. Electrode microstructure, CB distribution, porosity and electronic conductivity

The properties of dry anode layers prepared from conventional aqueous slurries and capillary suspensions with 2 vol% of octanol were compared, also including dry layers from capillary suspension slurries prepared at different mixing conditions. Finally, wet-on-wet coated double layers containing a regular slurry based bottom layer and a capillary suspension based top layer were fabricated and investigated as well.

3.2.1. Microstructural analysis

SEM investigations were carried out to analyze the microstructural properties of the composite electrodes. Besides the analysis of the electrode surface in terms of particle morphology and distribution of the conductive agent, electrode cross-sections were prepared using two different methods. To investigate the orientation of the active material particles in the electrode, cross-sections of the complete electrodes were prepared by embedding them in epoxy-resin, followed by polishing prior to SEM analysis. Moreover, the distribution and morphology of the CB agglomerates was analyzed using a FIB milling process. SEM images of the differently prepared electrodes are shown in Fig. 3. The overall distribution of CB is visible from the surface images shown in the upper line. In the conventionally prepared composite electrode (Fig. 3a) the CB particles are uniformly distributed covering large areas of the electrode surface. Even at low mixing speed which has been applied in the conventional preparation method, the CB particles are dispersed properly and form a conductive percolation network around the active material particles. Keeping the slurry mixing conditions constant, the addition of secondary fluid leads to the formation of large CB agglomerates (Fig. 3b). Due to the large surface area, the small radii and the accompanied small necks/gaps between adjacent CB particles, capillary bridges are preferentially formed between CB particles leading to large spherical agglomerates and thus an inhomogeneous distribution of the conductive agent. At higher mixing speeds, i.e. higher mechanical energy input, formation of large CB agglomerates is widely suppressed (Fig. 3c). The small agglomerates lead to a more homogeneous CB distribution and their location in the contact points between active material particles supports the formation of a percolating network (marked by arrows in Fig. 3c).

The cross-section SEM micrographs shown in Fig. 3 (middle row) reveal further consequences concerning the addition of octanol and the variation of mixing speed. The cross-section of the conventionally prepared electrode shows a preferential orientation of the plate-shaped particles parallel to the current collector leading to a rather dense microstructure (Fig. 3a). The large CB agglomerates formed in the capillary suspension based electrode act as spacer between active material particles. The absence of a preferential orientation results in a less dense packing, larger pores and thus an increased overall porosity of the layer (Fig. 3b). Applying an increased mixing speed during the addition of octanol results in a homogeneous distribution of CB particles and simultaneously suppresses the preferential orientation of active material particles preserving a highly porous microstructure (Fig. 3c). To confirm the conclusions regarding the distribution of the CB agglomerates deduced from SEM surface analysis, FIB-prepared cross-sections were investigated (see Fig. 3, bottom row). The uniformly dispersed CB particles in the conventionally processed electrode form rigid bridges between adjacent active material particles as marked in Fig. 3a. In contrast, the large CB agglomerates observed in the FIB-prepared cross-section in Fig. 3b serve as spacer between active material particles leading to an increased porosity. Finally, the formation of a percolating network of CB particles between the
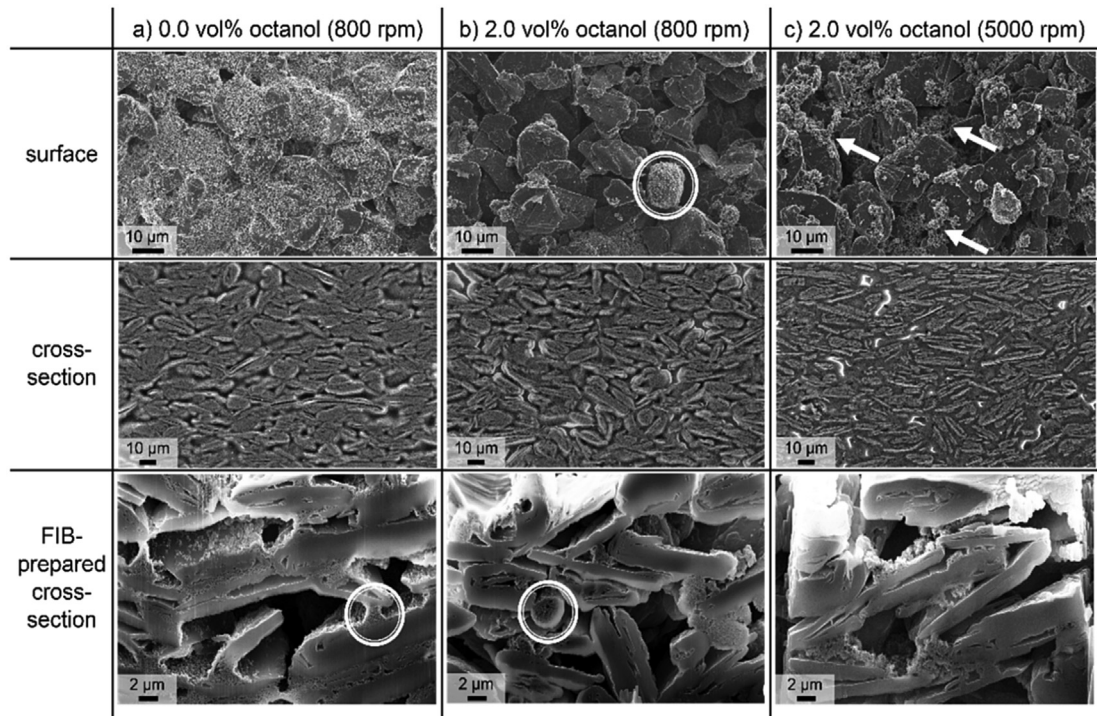
Fig. 3. SEM images of ultra-thick SLP30 electrodes made from slurries with different octanol content and prepared at different mixing speed (as quantified in brackets). a) 0.0 vol% octanol (800 rpm), b) 2.0 vol% octanol (800 rpm), and c) 2.0 vol% octanol (5000 rpm). Representative SEM images of the electrode surface (top), epoxy-resin embedded cross-sections (middle) and FIB-prepared cross-sections (bottom) are shown for the three processing routines.

active material particles while simultaneously preserving the high porosity was achieved by processing the capillary suspension at higher mixing speeds, as shown in Fig. 3c.

3.2.2. Hg-porosimetry and adhesion properties

The most important properties for all investigated single layers are summarized in Table 1. Referring to the active material, the mass loading was kept constant at 16.5 mg cm^{-2} (61 Ah m^{-2}) in order to ensure comparable conditions for electrochemical cycling. To show the influence of octanol addition on the porosity of the anodes, mercury intrusion measurements were executed. Coating and drying of conventional aqueous slurries leads to dry layers with a porosity of about 53% and a dry film thickness of about 195 μm. In contrast, after the addition of octanol a particle network resulting in considerably increased porosity and dry film thickness is formed at moderate mixing speed (porosity: 66%, dry film thickness: 250 μm). Increased energy input during dissolver mixing leads to partial de-agglomeration and a more uniform distribution of conductive agent but porosity and dry film thickness remain constant within experimental error (see Table 1).

Fig. 4 summarizes the measured pore size distributions as a function of the electrode preparation process. The addition of secondary fluid results in an altered pore structure since the average pore size is shifted to higher values while the pore size distribution broadens simultaneously. This effect becomes particularly distinct
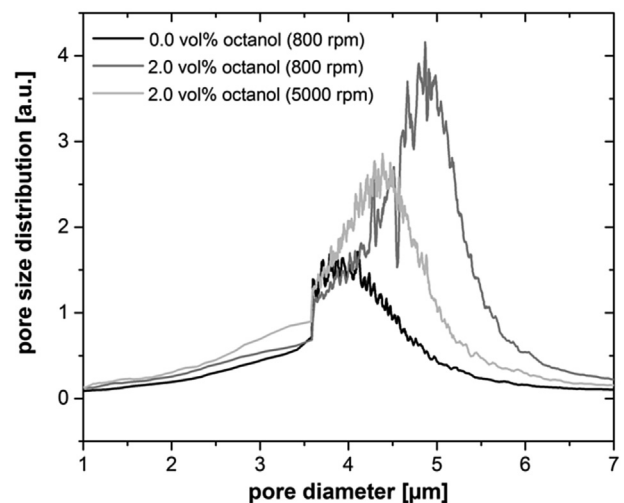

Fig. 4. Pore size distribution for conventionally processed and secondary fluid stabilized SLP30 based graphite electrodes obtained from mercury intrusion experiments.

Table 1
Characteristic numbers of dry ultra-thick electrodes based on conventionally prepared and octanol stabilized slurries.

Octanol fraction [vol%]	Dissolver speed (after octanol addition) [rpm]	Mass loading [mg cm^{-2}]	Specific area capacity [Ah m^{-2}]	Dry film thickness [μm]	Porosity (Hg intrusion) P [%]	Layer conductivity [S m^{-1}]
0	800	16.5 ± 0.5	61.4 ± 1.9	195 ± 5	53 ± 2	3119 ± 37
2	(800)	16.7 ± 0.5	62.1 ± 1.9	250 ± 5	66 ± 2	510 ± 12
2	(5000)	16.5 ± 0.5	61.4 ± 1.9	240 ± 5	63 ± 2	865 ± 27

for layers based on capillary suspensions stirred at low speed containing large CB agglomerates that serve as spacer elements. The partial disintegration of these agglomerates achieved by increased mixing speeds leads again to a reduced average pore diameter and a narrow pore size distribution.

Regarding the mechanical properties of dry layers 90° peel testing was applied. It was found that laminates based on octanol stabilized slurries show significantly lower mechanical stability in terms of peel force (line load) compared to layers based on regular slurries (2 vol% octanol, 800 rpm: 0.16 ± 0.06 N m^{-1}; 0 vol%, 800 rpm octanol: 3.08 ± 0.36 N m^{-1}) [36].

3.2.3. Electrode conductivity

Data in Table 1 based on the common four-point measuring technique reveals that the addition of octanol to the electrode slurry results in a drastic drop in the dry layer electronic conductivity by more than 80% compared to the conventional slurry based electrode prepared under similar conditions. This is attributed to the increase in dry film porosity and especially to the formation of large spherical CB agglomerates hindering the formation of conductive pathways within the composite electrode. However, Fig. 5 shows that the conductivity can be doubled by increasing the energy input during preparation of the capillary suspension type slurry. The porosity of the dry layer decreases only slightly with increasing energy input (as also shown in Fig. 5). Therefore, we conclude that the improved electronic conductivity is mainly due to a more uniform CB distribution as discussed above.

3.2.4. Electrochemical characterization

In order to evaluate the influence of the microstructure on the electrochemical performance CC-CP cycling was performed in common half-cells. Especially in case of ultra-thick composite electrodes the electrochemical performance is typically defined by intrinsic Li ion transport limitations governed by microstructural properties and the quality of the percolation network. Thus, besides constant current cycling at different C-rates, constant potential steps were implemented at the lower cut-off potential (0.02 V vs. Li/Li$^+$) to increase the overall reversibility of the charge/discharge capacity. Since the electrochemical cycling conditions (including the cut-off criterion for the CP steps) as well as the electrode mass loading are constant parameters, all variations in electrochemical performance can clearly be assigned to differences in the electrode microstructure.
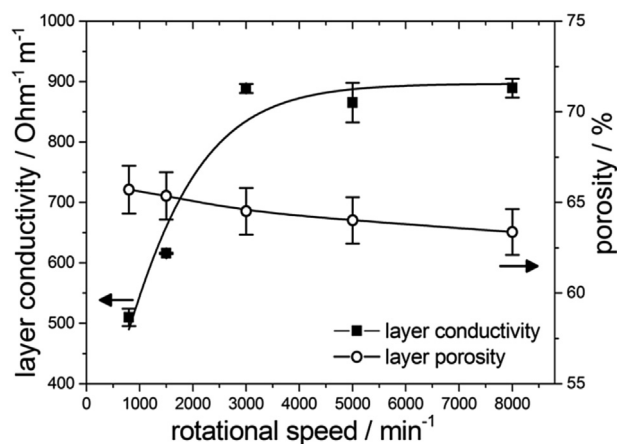

Fig. 5. Electronic conductivity and layer porosity for secondary fluid stabilized SLP30 composite electrodes based on slurries prepared with different (dissolver) mixing speeds. The octanol content was kept constant at 2.0 vol%.

3.2.5. Low C-rate cycling (overall cycle number 1–15)

As marked by the horizontal dashed line in Fig. 6a–c, all the electrodes reach the theoretical capacity of 372 mA h g^{-1} (C$_{theo}$(SLP30)) [47] at low C-rate cycling (0.1 C and 0.2 C) and subsequent CP step. These findings are not influenced by the preparation routine and the corresponding electrode microstructure. By differentiating between constant current and constant potential contributions to the overall specific discharge capacity the intrinsic transport limitation for ultra-thick composite electrodes can be investigated. For conventionally processed (Fig. 6a) and octanol stabilized electrodes prepared at low mixing speed (Fig. 6b) constant current (CC) cycling leads to a similar capacity of 325 mA h g^{-1} (0.1 C) and 175 mA h g^{-1} (0.2 C). In contrast, specific capacity data shown in Fig. 6c suggest that optimized microstructural properties in terms of a highly porous microstructure and an enhanced electronic percolation network are achieved by increasing the mixing speed (to 5000 rpm) after addition of octanol. In this case, low rate constant current (CC) cycling leads to increased capacities of 360 mA h g^{-1} (0.1 C) and 230 mA h g^{-1} (0.2 C), respectively. This result is a consequence of two effects: (i) the lithium ion transport kinetics is enhanced compared to conventionally prepared electrodes due to a higher porosity and (ii) the electronic conductivity is improved compared to the octanol stabilized electrode prepared at low mixing speed (800 rpm) due to a more homogeneous CB distribution (see also Fig. 3 and Table 1).

3.2.6. Medium C-rate cycling (overall cycle number 16–35) and final low C-rate cycling (cycles 36–38)

The constant current contribution to the overall capacity at 0.5 C is only slightly affected by the microstructure and CB distribution. Fig. 6a–c show that this CC-contribution to the specific capacity is 100 mAh g^{-1} for capillary suspension based electrodes (independent of the mixing speed) and 75 mAh g^{-1} for conventionally prepared electrodes. In general, slow electrode kinetics are attributed to common thickness effects in terms of intrinsic transport limitations and incomplete utilization of the active material within the electrode volume and can be overcome by implementation of a CP step (at 0.02 V vs. Li/Li$^+$) during cycling. For conventionally processed electrodes a significant increase in overall capacity to 300 mAh g^{-1} (81% of the theoretical capacity) can be recorded in the first cycle at 0.5 C. After 20 cycles at 0.5 C 250 mAh g^{-1} (67%) are remaining (Fig. 6a). In contrast, for octanol stabilized electrodes (2 vol%, 800 rpm and 5000 rpm) starting from 350 mAh g^{-1} (94% of theoretical capacity), even 320 mAh g^{-1} (86%) can be maintained after 20 cycles at 0.5 C including an additional CP step (compare Fig. 6b, c). Compared to conventional electrodes microstructural investigation of octanol stabilized electrodes reveals a much more pronounced open porosity. This facilitates electrolyte penetration and wetting of the active material particles leading to a higher utilization and increased specific capacity after medium C-rate cycling. Octanol stabilized electrode slurries treated with 5000 rpm lead to electrodes with a more homogeneous CB distribution accompanied by a higher electronic conductivity but a lower porosity compared to electrodes prepared at low mixing speed (see Table 1, Figs. 3b and 5). Consequently, in the case of octanol stabilized electrodes, enhanced electrode kinetics and Li ion transport properties come into effect because (i) the value of open porosity, the degree of electrolyte wetting and utilization of active material and (ii) the homogeneity of CB distribution and the formation of electronic conductive pathways are improved. Since these two effects are competitive with regard to the overall electrochemical performance octanol stabilized electrodes show a similar medium C-rate performance.

Increasing the C-rate from 0.2 C to 0.5 C, conventionally prepared electrodes show a severe capacity drop (see Fig. 6a). It is
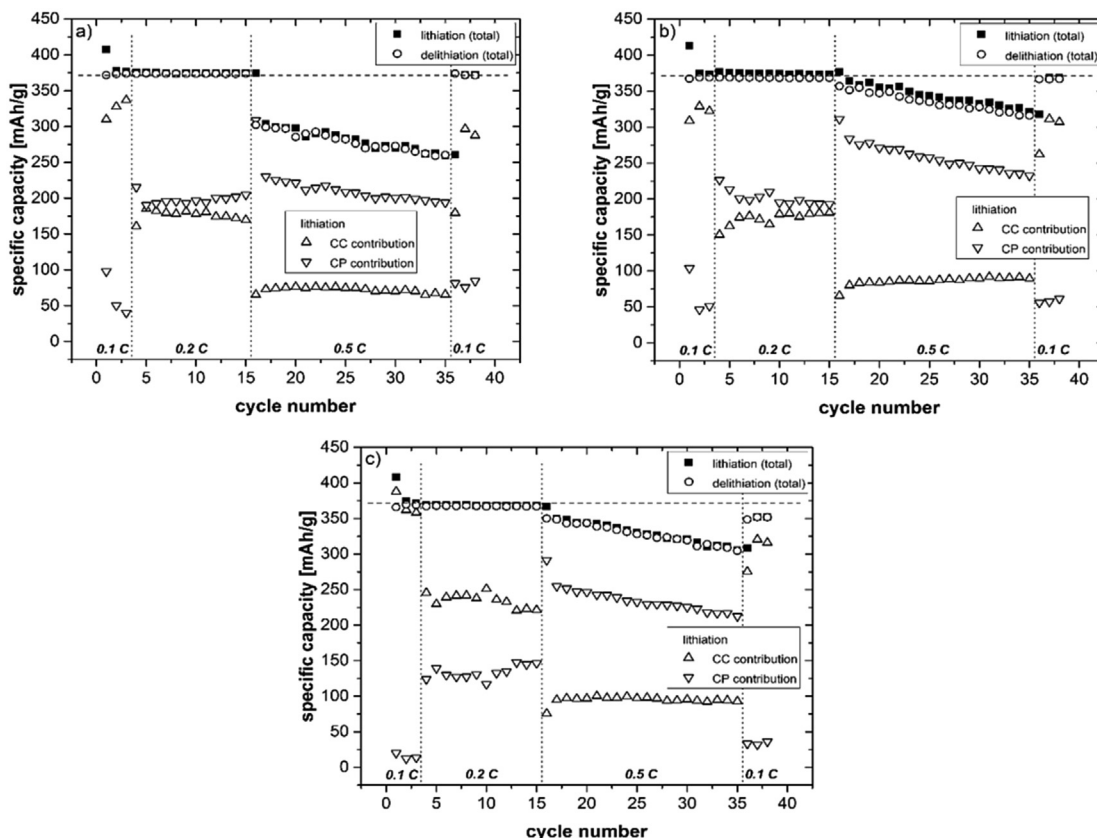
Fig. 6. Constant current-constant potential (CC-CP) cycling of ultra-thick composite electrodes prepared with a) 0.0 vol% octanol at a rotational speed of 800 rpm, b) 2.0 vol% octanol (800 rpm), and c) 2.0 vol% octanol (5000 rpm). Constant current (CC) and constant potential (CP) contributions to overall capacity are plotted separately for the lithium insertion processes. The theoretical capacity of SLP30 is marked by the horizontal dashed line; vertical dotted lines separate cycles operated at different C-rates.

likely that this effect correlates with the electrode microstructure. Compared to the pronounced open porosity in case of octanol stabilized electrodes, conventionally prepared samples suffer from ion transport limitations at higher C-rates leading to lower overall capacities (see Fig. 6a).

While the constant current contribution to the overall capacity remains constant, capacity fading only affects the capacity contribution after the CP step. Since the slope of capacity fading (capacity as function of cycle number, 0.5 C) does not correlate with process parameters and the individual microstructure of the electrodes the capacity loss might be attributed to side reactions at the lower cut-off potential, such as electrolyte decomposition or Li dendrite formation.

As a consequence of relaxation processes the initial low-rate capacity and therefore the theoretical capacity for SLP30 can almost be retained during subsequent cycling at 0.1 C for both conventionally prepared and octanol stabilized electrodes.

3.2.7. Double electrode layer investigation

In order to further optimize the microstructure of ultra-thick SLP30 composite electrodes, wet-on-wet slot die coating was applied to build up an electrode with staged porosity. An octanol stabilized slurry was coated on top of a conventionally prepared one to combine optimum adhesion properties with a highly porous layer for improved electrolyte penetration. The octanol stabilized slurry was mixed at 5000 rpm to achieve sufficient CB distribution. Analysis of SEM cross-sections reveals that the resulting dry layer (dry film thickness: 170 µm ± 5 µm) exhibits a peculiar microstructure. As summarized in Fig. 7 the SLP30 particle orientation

significantly differs between the top and bottom part. The corresponding differential and cumulative distributions of particle orientation relative to the metal foil (defined as q_0 and Q_0) are presented in Fig. 7a, b. These numbers were derived from SEM cross-section micrographs as exemplarily illustrated in Fig. 7c. The orientation of the plate-shaped active material particles is rather parallel to the substrate in the bottom part next to the current collector (compare Fig. 7b), whereas in the top layer the particle orientation is more random (Fig. 7a). The different particle orientation is consistent with the microstructure observed for corresponding single layers (compare Fig. 3). This also indicates a different, layer dependent porosity. As shown by mercury intrusion measurements, the mean porosity of the double layer system is (61 ± 2)%. This value is within the range between (53 ± 2)% for a conventionally processed and (63 ± 2)% for a secondary fluid stabilized layer (see Table 1). The measured layer conductivity of (1567 ± 90) S m^{-1} is also within the conductivity limits defined by the single layers (see Table 1).

The porosity gradient within the electrode cross-section is supposed to positively affect the Li ion transport properties during electrochemical cycling. Preliminary electrochemical CC-CP investigations seem to support this assumption as the overall capacity reaches 360 mAh g^{-1} even at 0.5C (see Fig. 8). It has to be emphasized that this particular double layer mass loading was (12.5 ± 0.5) mg cm^{-2} instead of (16.5 ± 0.5) mg cm^{-2} chosen for the single layers as discussed above. This deviation in mass loading basically is a consequence of slurry processing, thus the application of different coating techniques (doctor blade coating for single layers and slot die coating for double layer formation) is considered
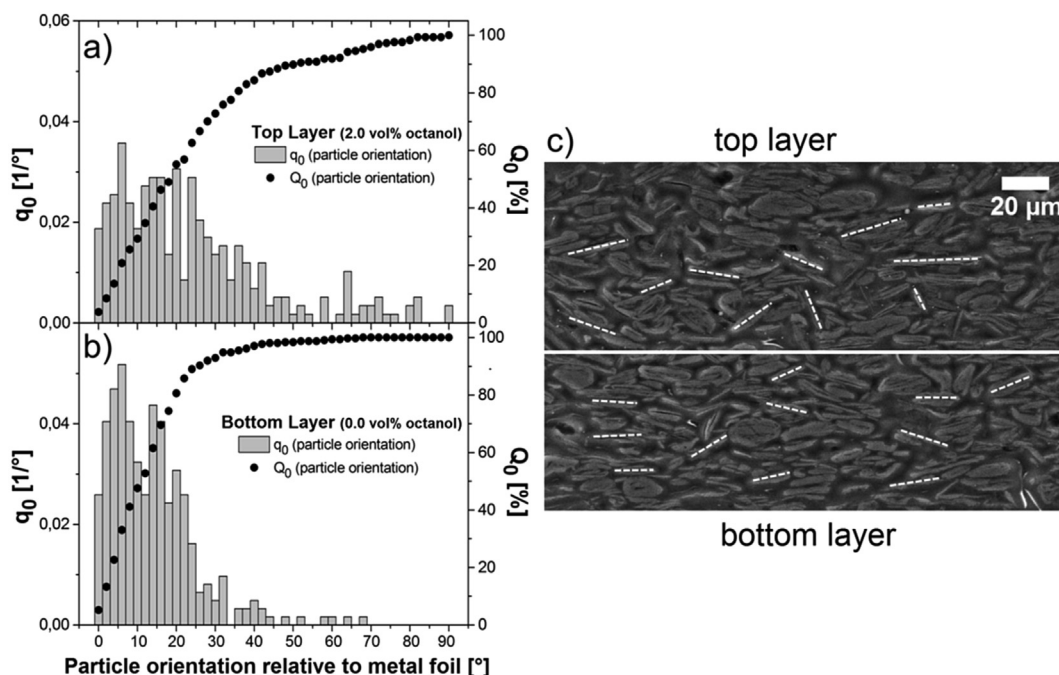
Fig. 7. Histograms showing the particle orientation relative to the current collector plane for the octanol stabilized top layer (a) and the bottom layer obtained from a conventional slurry (b). (c) illustrates the evaluation of particle orientation by graphical analysis of a SEM cross-section micrograph.
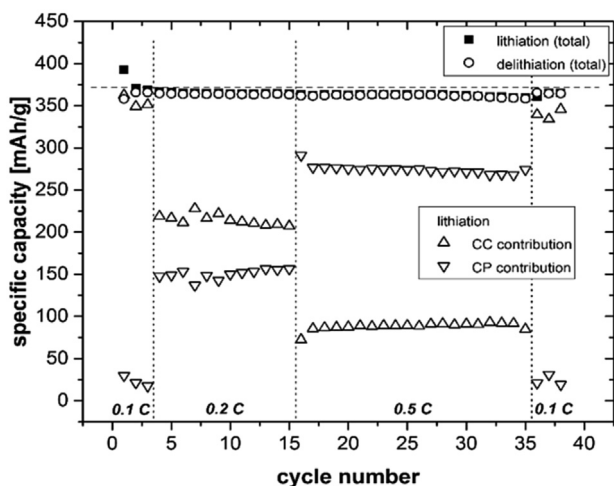

Fig. 8. Constant current-constant potential (CC-CP) cycling of a double electrode layer composite electrode system consisting of a conventionally prepared slurry (0.0 vol% octanol, 800 rpm) next to the current collector and an octanol stabilized layer (2.0 vol% octanol, 5000 rpm) on top. Constant current (CC) and constant potential (CP) contributions to overall capacity are plotted separately for lithium insertion processes. The theoretical capacity of SLP30 is marked by the horizontal dashed line; vertical dotted lines separate cycles operated at different C-rates.

to be investigated and adjusted in future experiments.

In order to elucidate the influence of electrode microstructure on the Li ion transport kinetics, both double layer electrode components (0.0 vol% octanol, 800 rpm and 2.0 vol% octanol, 5000 rpm) were additionally prepared as single layers with a corresponding mass loading of (12.5 ± 0.5) mg cm^{-2}. As shown in Fig. SI1 (see supporting information), the electrochemical properties are in agreement with the data depicted in Fig. 7a, c. The beneficial effect of staged porosity regarding the Li ion transport properties becomes obvious comparing the double layer electrode and the

octanol stabilized single layer. Both systems reveal comparable overall capacities (compare Fig. 8 and Fig. SI1b) but since the double layer is more densely packed (due to staged porosity) these electrodes exhibit a higher volumetric energy density.

4. Conclusion

In this study a novel and simple processing route to prepare ultra-thick electrodes suitable for low cost production and high energy density battery cell applications is introduced. The capillary suspension formulation concept already established to control the pore size and the structure of sintered membranes [37] is successfully applied to adjust microstructure and porosity of water based graphite anodes. Keeping the total number of processing steps constant, the preparation routine can be easily implemented in conventional industrial slurry processing procedures. Wet film stabilization, i.e. drastically increased viscosity at low shear stress as a consequence of the addition of octanol as secondary fluid, results in beneficial slurry processing properties. This includes the applicability in high speed coating operations and the replacement of additional more sophisticated binder additives like e.g., latex particles. The octanol-assisted processing enables the preparation of wet films with homogeneous thickness and sharp edges [36] resulting in uniform dry film thicknesses of up to 250 μm. As verified by mercury intrusion measurements, slurry preparation based on capillary suspensions is suitable to tailor the microstructure of a dry composite electrode since porosity and pore size distribution can be controlled by the amount of added secondary fluid. As proven by FIB/SEM investigations the addition of the secondary fluid results in the formation of large spherical carbon black agglomerations in the dry composite electrode. By increasing the mechanical energy input during mixing a uniform CB distribution was achieved maintaining an open porosity. In general, the electrochemical performance of a composite electrode strongly depends on the distribution of the conductive agent and the resulting porosity of the dry layer. CC-CP cycling was performed in

half-cells (vs. Lithium metal) to figure out the influence of secondary fluid stabilization on the electrode performance. Starting from conventionally prepared (thick) electrodes, the optimization of carbon black distribution and thus the peculiar pore structure is essential to improve the electrochemical performance of ultrathick electrodes. As expected, electrochemical cycling of SLP30 at low C-rates always leads to the theoretical capacity, independent of the preparation routine. The analysis of the overall capacity in terms of constant current and constant potential capacity contributions elucidates the improved electrochemical performance of octanol stabilized electrodes due to their unique microstructure. In particular, an increased constant current capacity contribution clearly indicates improved electrochemical properties of octanol stabilized electrodes.

Beyond that, a more sophisticated approach is proved by applying the capillary suspension formulation concept to successfully prepare an electrode with staged porosity via wet-on-wet coating. For a slightly reduced mass loading an outstanding capacity of about 360 mA h g^{-1} can be obtained at 0.5 C.

In general, using capillary suspensions to prepare electrodes gives rise to a broad field of opportunities regarding the optimization of slurry formulations. In this context the capillary suspension phenomenon may be used, e.g. for an efficient, targeted deposition of the binder using the secondary fluid as carrier [40]. The next step towards the technical implementation of this technology will be the transfer from laboratory to pilot plant covering industrial coating techniques, such as e.g. multilayer slot die coating.

Acknowledgements

Appendix A. Supplementary data

Supplementary data related to this article can be found at http://dx.doi.org/10.1016/j.jpowsour.2016.07.102.

References

[1] R. Wagner, N. Preschitschek, S. Passerini, J. Leker, M. Winter, Current research trends and prospects among the various materials and designs used in lithium-based batteries, J. Appl. Electrochem. 43 (2013) 481–496, http://dx.doi.org/10.1007/s10800-013-0533-6.

[2] P. Bieker, M. Winter, Was braucht man für eine Super-Batterie? Chem. Unserer Zeit 50 (2016) 26–33, http://dx.doi.org/10.1002/ciuz.201500713.

[3] S.S. Zhang, K. Xu, T.R. Jow, Evaluation on a water-based binder for the graphite anode of Li-ion batteries, J. Power Sources 138 (2004) 226–231, http://dx.doi.org/10.1016/j.jpowsour.2004.05.056.

[4] J. Drofenik, M. Gaberscek, R. Dominko, F.W. Poulsen, M. Mogensen, S. Pejovnik, et al., Cellulose as a binding material in graphitic anodes for Li ion batteries: a performance and degradation study, Electrochim. Acta 48 (2003) 883–889, http://dx.doi.org/10.1016/S0013-4686(02)00784-3.

[5] J.-H. Lee, U. Paik, V.A. Hackley, Y.-M. Choi, Effect of carboxymethyl cellulose on aqueous processing of natural graphite negative electrodes and their electrochemical performance for lithium batteries, J. Electrochem. Soc. 152 (2005) A1763–A1769, http://dx.doi.org/10.1149/1.1979214.

[6] J.H. Lee, S. Lee, U. Paik, Y.M. Choi, Aqueous processing of natural graphite particulates for lithium-ion battery anodes and their electrochemical performance, J. Power Sources 147 (2005) 249–255, http://dx.doi.org/10.1016/j.jpowsour.2005.01.022.

[7] H. Buqa, M. Holzapfel, F. Krumeich, C. Veit, P. Novák, Study of styrene butadiene rubber and sodium methyl cellulose as binder for negative electrodes in

[8] G. Jeong, Y.-U. Kim, H. Kim, Y.-J. Kim, H.-J. Sohn, Prospective materials and applications for Li secondary batteries, Energy Environ. Sci. 4 (2011) 1986–2002, http://dx.doi.org/10.1039/c0ee00831a.

[9] S.F. Lux, F. Schappacher, A. Balducci, S. Passerini, M. Winter, Low cost, environmentally benign binders for lithium-ion batteries, J. Electrochem. Soc. 157 (2010) A320–A325, http://dx.doi.org/10.1149/1.3291976.

[10] M. Park, X. Zhang, M. Chung, G.B. Less, A.M. Sastry, A review of conduction phenomena in Li-ion batteries, J. Power Sources 195 (2010) 7904–7929, http://dx.doi.org/10.1016/j.jpowsour.2010.06.060.

[11] S.-L. Chou, Y. Pan, J.-Z. Wang, J.-K. Liu, S.-X. Dou, Small things make a big difference: binder effects on the performance of Li and Na batteries, Phys. Chem. Chem. Phys. 16 (2014) 20347–20359, http://dx.doi.org/10.1039/C4CP02475C.

[12] H. Zheng, J. Li, X. Song, G. Liu, V.S. Battaglia, A comprehensive understanding of electrode thickness effects on the electrochemical performances of Li-ion battery cathodes, Electrochim. Acta 71 (2012) 258–265, http://dx.doi.org/10.1016/j.electacta.2012.03.161.

[13] X. Qi, B. Blizanac, A. DuPasquier, A. Lal, P. Niehoff, T. Placke, et al., Influence of thermal treated carbon black conductive additive on the performance of high voltage spinel Cr-Doped LiNi0.5Mn1.5O4 composite cathode electrode, J. Electrochem. Soc. 162 (2015) A339–A343, http://dx.doi.org/10.1149/2.0401503jes.

[14] X. Qi, B. Blizanac, A. DuPasquier, P. Meister, T. Placke, M. Oljaca, et al., Investigation of PF6(-) and TFSI(-) anion intercalation into graphitized carbon blacks and its influence on high voltage lithium ion batteries, Phys. Chem. Chem. Phys. 16 (2014) 25306–25313, http://dx.doi.org/10.1039/c4cp04113e.

[15] X. Qi, B. Blizanac, A. Dupasquier, M. Oljaca, J. Li, M. Winter, Understanding the influence of conductive carbon additives surface area on the rate performance of LiFePO4 cathodes for lithium ion batteries, Carbon N. Y. 64 (2013) 334–340, http://dx.doi.org/10.1016/j.carbon.2013.07.083.

[16] K.M. Abraham, Prospects and limits of energy storage in batteries, J. Phys. Chem. Lett. 6 (2015) 830–844, http://dx.doi.org/10.1021/jz5026273.

[17] R. de Levie, On porous electrodes in electrolyte solutions, Electrochim. Acta 8 (1963) 751–780, http://dx.doi.org/10.1016/0013-4686(64)85015-5.

[18] S. Golmon, K. Maute, M.L. Dunn, Numerical modeling of electrochemical-mechanical interactions in lithium polymer batteries, Comput. Struct. 87 (2009) 1567–1579, http://dx.doi.org/10.1016/j.compstruc.2009.08.005.

[19] J. Illig, J.P. Schmidt, M. Weiss, A. Weber, E. Ivers-Tiffée, Understanding the impedance spectrum of 18650 LiFePO4-cells, J. Power Sources 239 (2013) 670–679, http://dx.doi.org/10.1016/j.jpowsour.2012.12.020.

[20] N. Ogihara, S. Kawauchi, C. Okuda, Y. Itou, Y. Takeuchi, Y. Ukyo, Theoretical and experimental analysis of porous electrodes for lithium-ion batteries by electrochemical impedance spectroscopy using a symmetric cell, J. Electrochem. Soc. 159 (2012) A1034–A1039, http://dx.doi.org/10.1149/2.057207jes.

[21] Y. Orikasa, Y. Gogyo, H. Yamashige, M. Katayama, K. Chen, T. Mori, et al., Ionic conduction in lithium ion battery composite electrode governs cross-sectional reaction distribution, Sci. Rep. 6 (2016) 26382, http://dx.doi.org/10.1038/srep26382.

[22] J. Landesfeind, J. Hattendorff, A. Ehrl, W.A. Wall, H.A. Gasteiger, Tortuosity determination of battery electrodes and separators by impedance spectroscopy, J. Electrochem. Soc. 163 (2016) A1373–A1387, http://dx.doi.org/10.1149/2.1141607jes.

[23] M. Wang, J. Li, X. He, H. Wu, C. Wan, The effect of local current density on electrode design for lithium-ion batteries, J. Power Sources 207 (2012) 127–133, http://dx.doi.org/10.1016/j.jpowsour.2011.12.063.

[24] S. Yu, S. Kim, T.Y. Kim, J.H. Nam, W. Il Cho, Model prediction and experiments for the electrode design optimization of LiFePO4/graphite electrodes in high capacity lithium-ion batteries, Bull. Korean Chem. Soc. 34 (2013) 79–88, http://dx.doi.org/10.5012/bkcs.2013.34.1.79.

[25] W. Haselrieder, Impact of the calendering process on the interfacial structure and the related electrochemical performance of secondary lithium-ion batteries, ECS Trans. 50 (2013) 59–70, http://dx.doi.org/10.1149/05026.0059ecst.

[26] M. Lanz, P. Novák, DEMS study of gas evolution at thick graphite electrodes for lithium-ion batteries: the effect of γ-butyrolactone, J. Power Sources 102 (2001) 277–282, http://dx.doi.org/10.1016/S0378-7753(01)00826-6.

[27] K.C. Kil, U. Paik, Lithium salt of carboxymethyl cellulose as an aqueous binder for thick graphite electrode in lithium ion batteries, Macromol. Res. 23 (2015) 719–725, http://dx.doi.org/10.1007/s13233-015-3094-1.

[28] N. Ogihara, Y. Itou, T. Sasaki, Y. Takeuchi, Impedance spectroscopy characterization of porous electrodes under different electrode thickness using a symmetric cell for high-performance lithium-ion batteries, J. Phys. Chem. C 119 (2015) 4612–4619, http://dx.doi.org/10.1021/jp512564f.

[29] S. Golmon, K. Maute, M.L. Dunn, Multiscale design optimization of lithium ion batteries using adjoint sensitivity analysis, Int. J. Numer. Methods Eng. 92 (2012) 475–494, http://dx.doi.org/10.1002/nme.

[30] S. Golmon, K. Maute, M.L. Dunn, A design optimization methodology for Li+ batteries, J. Power Sources 253 (2014) 239–250, http://dx.doi.org/10.1016/j.jpowsour.2013.12.025.

[31] M. Stieß, Mechanische Verfahrenstechnik - Partikeltechnologie 1, Springer, Berlin, 2009, http://dx.doi.org/10.1007/978-3-540-32552-9.

[32] H. Kim, R.C.Y. Auyeung, A. Piqué, Laser-printed thick-film electrodes for solid-state rechargeable Li-ion microbatteries, J. Power Sources 165 (2007)

413–419, http://dx.doi.org/10.1016/j.jpowsour.2006.11.053.

[33] J. Pröll, H. Kim, A. Piqué, H.J. Seifert, W. Pfleging, Laser-printing and femtosecond-laser structuring of LiMn2O 4 composite cathodes for Li-ion microbatteries, J. Power Sources 255 (2014) 116–124, http://dx.doi.org/10.1016/j.jpowsour.2013.12.132.

[34] J.H. Pikul, H. Gang Zhang, J. Cho, P.V. Braun, W.P. King, High-power lithium ion microbatteries from interdigitated three-dimensional bicontinuous nano-porous electrodes, Nat. Commun. 4 (2013) 1732, http://dx.doi.org/10.1038/ncomms2747.

[35] E. Koos, N. Willenbacher, Capillary forces in suspension rheology, Science 331 (2011) 897–900, http://dx.doi.org/10.1126/science.1199243.

[36] B. Bitsch, J. Dittmann, M. Schmitt, P. Scharfer, W. Schabel, N. Willenbacher, A novel slurry concept for the fabrication of lithium-ion battery electrodes with beneficial properties, J. Power Sources 265 (2014) 81–90, http://dx.doi.org/10.1016/j.jpowsour.2014.04.115.

[37] J. Dittmann, E. Koos, N. Willenbacher, Ceramic capillary suspensions: novel processing route for macroporous ceramic materials, J. Am. Ceram. Soc. 96 (2013) 391–397, http://dx.doi.org/10.1111/jace.12126.

[38] J. Dittmann, N. Willenbacher, Micro structural investigations and mechanical properties of macro porous ceramic materials from capillary suspensions, J. Am. Ceram. Soc. 97 (2014) 3787–3792, http://dx.doi.org/10.1111/jace.13184.

[39] J. Maurath, J. Dittmann, N. Schultz, N. Willenbacher, Fabrication of highly porous glass filters using capillary suspension processing, Sep. Purif. Technol. 149 (2015) 470–478, http://dx.doi.org/10.1016/j.seppur.2015.06.022.

[40] J. Dittmann, J. Maurath, B. Bitsch, N. Willenbacher, Highly porous materials with unique mechanical properties from smart capillary suspensions, Adv. Mater 28 (2015) 1689–1696, http://dx.doi.org/10.1002/adma.201504910.

[41] J.P. Olivier, M. Winter, Determination of the absolute and relative extents of basal plane surface area and "non-basal plane surface" area of graphites and their impact on anode performance in lithium ion batteries, J. Power Sources 97–8 (2001) 151–155. <Go to ISI>://000169836000033.

[42] M.E. Spahr, D. Goers, A. Leone, S. Stallone, E. Grivei, Development of carbon conductive additives for advanced lithium ion batteries, J. Power Sources 196 (2011) 3404–3413, http://dx.doi.org/10.1016/j.jpowsour.2010.07.002.

[43] B. Bitsch, N. Willenbacher, V. Wenzel, S. Schmelzle, H. Nirschl, Einflüsse der mechanischen Verfahrenstechnik auf die Herstellung von Elektroden für Lithium-Ionen-Batterien, Chem. Ing. Tech. 87 (2015) 466–474, http://dx.doi.org/10.1002/cite.201400093.

[44] E. Koos, Capillary suspensions: particle networks formed through the capillary force, Curr. Opin. Colloid Interface Sci. 19 (2014) 575–584, http://dx.doi.org/10.1016/j.cocis.2014.10.004.

[45] B. Bitsch, B. Braunschweig, N. Willenbacher, Interaction between polymeric additives and secondary fluids in capillary suspensions, Langmuir 32 (2016) 1440–1449, http://dx.doi.org/10.1021/acs.langmuir.5b03861.

[46] E. Koos, W. Kannowade, N. Willenbacher, Restructuring and aging in a capillary suspension, Rheol. Acta 53 (2014) 947–957, http://dx.doi.org/10.1007/s00397-014-0805-z.

[47] C. Daniel, Materials and processing for lithium-ion batteries, JOM 60 (2008) 43–48, http://dx.doi.org/10.1007/s11837-008-0116-x.